Influence of the Template Layer on the Structure and Ferroelectric Properties of PbZr$_{0.52}$Ti$_{0.48}$O$_3$ Films

Philip Lucke,* Mohammadreza Nematollahi, Muharrem Bayraktar, Andrey E. Yakshin, Johan E. ten Elshof, and Fred Bijkerk

Read Online

ACCESS | Metrics & More | Article Recommendations

ABSTRACT: The microstructure of the PbZr$_{0.52}$Ti$_{0.48}$O$_3$ (PZT) films is known to influence the ferroelectric properties, but so far mainly the effect of the deposition conditions of the PZT has been investigated. To our knowledge, the influence of the underlying electrode layer and the mechanisms leading to changes in the PZT microstructure have not been explored. Using LaNiO$_3$ (LNO) as the bottom electrode material, we investigated the evolution of the PZT microstructure and ferroelectric properties for changing LNO pulsed-laser deposition conditions. The explored deposition conditions were the O$_2$ pressure, total pressure, and thickness of the electrode layer. Increasing both the O$_2$ pressure and the thickness of the electrode layer changes the growth of PZT from a smooth, dense film to a rough, columnar film. We explain the origin of the change in PZT microstructure as the increased roughness of the electrode layer in relaxing the misfit strain. The strain relaxation mechanism is evidenced by the increase in the crystal phase with bulk LNO unit cell dimensions in comparison to the crystal phase with substrate-clamped unit cell dimensions. We explain the change from a dense to a columnar microstructure as a result of the change in the growth mode from Frank−van der Merwe to Stranski−Krastanov. The ferroelectric properties of the columnar films are improved compared to those of the smooth, dense films. The ability to tune the ferroelectric properties with the microstructure is primarily relevant for ferroelectric applications such as actuators and systems for energy harvesting and storage.
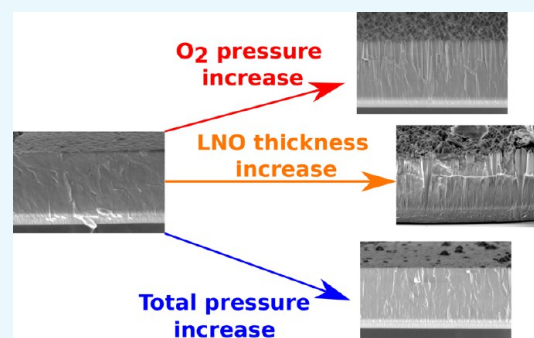
INTRODUCTION

Ferroelectric thin films are of high interest for applications such as ferroelectric memories and in microelectromechanical systems as sensors and actuators.[1−10] In particular, PbTi$_{1−x}$Zr$_x$O$_3$ (PZT) is favored because of its outstanding ferroelectric and piezoelectric properties. These functional properties of PZT thin films are highly dependent on several material properties, such as the stoichiometry, crystal orientation, and microstructure. The most favorable properties of PZT are found in the x = 0.48 morphotropic phase boundary (MPB) composition.[11−14] It has been shown theoretically[15,16] and experimentally[17−19] that the PZT grown in the (001) orientation, which is the out-of-plane direction, exhibits a higher functional response than do other orientations, hence the PZT films have been initially grown on lattice-matched SrTiO$_3$ substrates to promote such oriented growth.[20,21] To grow (001)-oriented PZT on low-cost substrates such as Si, glass, and metals, several buffer layers have been explored.[22−25] In particular, it has been shown that chemically synthesized unit-cell-thick oxide nanosheets can be used to achieve the desired out-of-plane crystal orientation on silicon and glass substrates.[26−31] Given the right stoichiometry

and orientation, the ferroelectric response is further affected by the microstructure of the film, which is affected by the grain size and domain structure.[3,32,33] The film microstructure also influences the application-relevant piezoelectric properties by influencing the elastic parameters of the film.[34−40] Therefore, it is important to explore the methods that allow the film microstructure and consequent influences on the film's functional properties to be controlled.

The influence of the microstructure on the functional properties of the deposited films has been studied using various deposition techniques. Investigations of chemical-solution-deposited PZT films show that dense films can be produced by process optimization and multiple-step deposition.[41,42] In magnetron-sputtered PZT films, dense films have been reported when matching template layers[43−46] and a columnar

Table 1. Sample List and Their Deposition Parameters, along with the Measured Thicknesses and the RMS Surface Roughness

	LNO					PZT	
sample	O_2 pressure (mbar)	Ar pressure (mbar)	pulses	thickness (nm)	roughness RMS (nm)	thickness (nm)	roughness RMS (nm)
A1	0.10		3960	90		1000	7.2 ± 3.6
A2	0.25		3960	100		1000	11.1 ± 2.6
A3	0.50		3960	95		1100	20.3 ± 1.8
A4	0.80		3960	95		1300	23.4 ± 3.5
B1	0.10	0.70	3960	96		1100	13.9 ± 3.6
C1	0.10		10 560	250		1050	24.9 ± 1.8
C2	0.50		7800	240		1200	26.3 ± 1.2
D1	0.10		3960	85	0.5		
D2	0.80		3960	120	2.3		
D3	0.10	0.70	3960	83	0.8		
D4	0.10		10 560	190	1.5		

microstructure has been reported for fast-cooled low-temperature depositions.[47] Pulsed laser deposition (PLD) is a proven technique for high-crystal-quality growth with an important additional parameter, i.e., the laser repetition frequency. It has been shown that a low laser repetition frequency helps in producing dense films and increasing the frequency can convert the film microstructure from dense to columnar.[38,40] To the best of our knowledge, the changes in microstructure and ferroelectric properties have so far been explored only with regard to the deposition conditions of the PZT, even though it is well known that the template layer has an influence on the microstructure and thus also on the ferroelectric properties of the subsequent layers.

From an application point of view, it is known that the film microstructure influences the ferroelectric and piezoelectric properties. In energy storage devices, for example, a low remnant and a high maximum polarization in combination with minimal hysteresis are desired to increase the amount of recoverable energy.[48] Because these properties are, among other things, dependent on the film microstructure, investigating the influence of the template layer on the ferroelectric film in terms of microstructure and ferroelectric properties is of interest. The influence of the template layer is also of interest for energy-harvesting devices because the piezoelectric properties of the film are influenced by the microstructure. Any improvement in the piezoelectric properties can directly lead to an improvement in the figures of merit of the energy-harvesting devices.[49,50] Furthermore, the ability to control the mode of operation between bending type (d_{31} mode) and piston type (d_{33} mode) by tuning the microstructure is attractive for modern microelectromechanical actuators.[4,19,51]

Here, we investigate the effect of the deposition conditions of the template layer, $LaNiO_3$ (LNO), on the microstructure and ferroelectric properties of the subsequently deposited PZT layer. The deposition conditions that were explored were the gas pressure and the thickness of the template layer while the subsequent PZT deposition conditions, including the laser repetition frequency, were kept constant for all samples.

■ EXPERIMENTAL DETAILS

Film Deposition and Fabrication. All samples were deposited by PLD with a KrF excimer Laser (Lambda Physik COMPex Pro 205, wavelength 248 nm, pulse duration 20 ns, maximum repetition frequency 50 Hz) on Si substrates that were precoated with $Ca_2Nb_3O_{10}$ (CNO) nanosheets using Langmuir–Blodgett deposition. The in-plane lattice parameters of the CNO nanosheets (3.86 Å) and LNO (3.84 Å) are close

to each other, which promotes the (001) orientation of the LNO and additional PZT layers.[26,30,52] More information on the nanosheets can be found in Nguyen et al.[30] All depositions were performed in a chamber with a base pressure of below 2.5 × 10⁻⁵ mbar. During the deposition of all films, the substrate temperature was kept constant at 600 °C. For all samples, the LNO was ablated from a stoichiometric target (Kurt J. Lesker) with a laser spot size of 3 mm², a fluence of 2.25 J cm⁻², a repetition frequency of 4 Hz, and a substrate-to-target distance of 60 mm. Four sets of samples were fabricated by varying the O_2 pressure (set A), introducing a buffer gas (set B), and increasing the thickness of the LNO in the LNO\PZT heterostructure (set C) and in order to study the LNO template layer in detail for sole LNO layers (set D), as summarized in Table 1. The starting O_2 pressure during the LNO deposition was taken from the literature,[38] and a maximum pressure of 0.8 mbar was the limit of the experimental setup. The starting thickness of LNO layers was selected to be around 100 nm, a common thickness for oxide electrodes for thick PZT films.[33] The PZT was subsequently deposited on top of the LNO film without breaking the vacuum. The PZT layer was deposited from an MPB $PbZr_{0.52}Ti_{0.48}O_3$ ceramic target (homemade) at a pressure of 0.1 mbar O_2, a laser spot size of 3 mm², a flauence of 2.5 J cm⁻², a repetition frequency of 50 Hz, and a substrate-to-target distance of 55 mm as in the literature.[38] After the deposition, the samples were cooled to room temperature at a cooling rate of 8 °C min⁻¹ at 1 mbar O_2 pressure. In the set D samples, only the lowest and highest ranges of the parameters were investigated. For ferroelectric measurements of the LNO\PZT heterostructures (sets A−C), a 100-nm-thick platinum (Pt) layer was deposited on top of the PZT layer by sputtering. The deposited Pt layer was patterned and structured into 200 × 200 μm^2 top electrodes using a standard photolithography lift-off process. The bottom electrode was contacted by the use of silver glue on the side of the sample.

Analysis and Characterization. The crystallographic properties of sets A−C were analyzed using θ−2θ scans with an X-ray diffractometer (XRD) system (PANalytical X'Pert). The film surface was investigated by means of atomic force microscopy (AFM, Bruker Dimension ICON), and the root-mean-square (RMS) surface roughness was calculated. The RMS roughness values for sets A−C correspond to the average value taken from five 1 × 1 μm^2 areas on the smooth nanosheet-coated regions. The AFM images of set D covered only nanosheet-coated 1.5 × 1.5 μm^2 areas, and the RMS
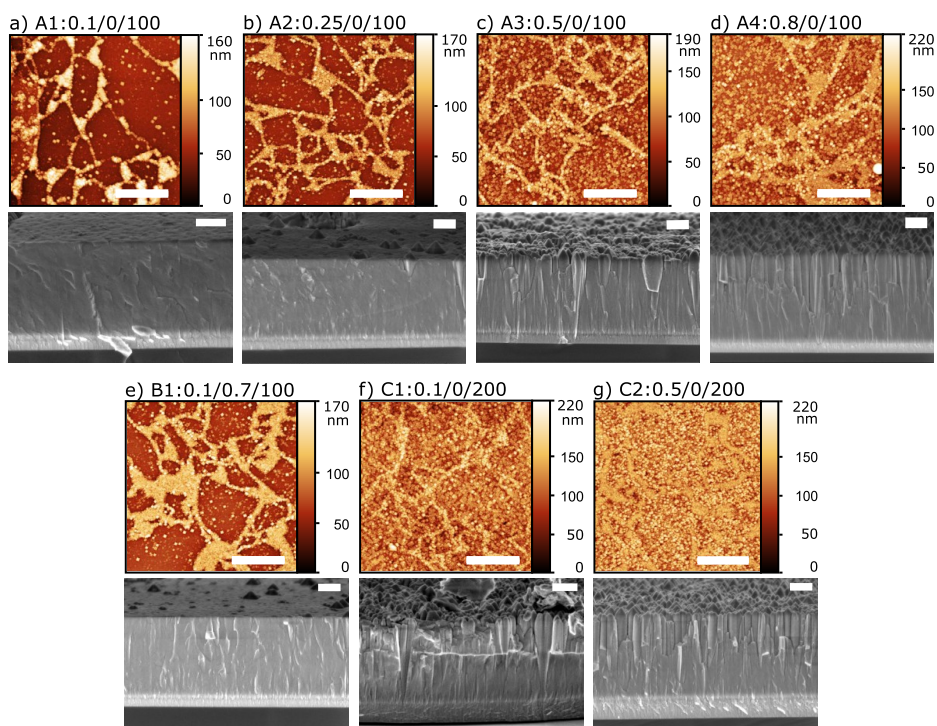
Figure 1. (a−g) AFM surface scans and SEM cross sections for LNO\PZT samples. The deposition conditions are given at the top of each subfigure with the following coding: O2 p.p./Ar p.p./LNO thickness (nm) sample ID. The scale bar in the AFM represents 3 μm (10 × 10 μm^2 area), and that in the SEM corresponds to 300 nm.

values were calculated over the complete area. The cross-sectional microstructure and film thicknesses were investigated by high-resolution scanning electron microscopy (HR-SEM, Zeiss Merlin 1550). The polarization hysteresis measurements were performed with a ferroelectric analyzer (AixACCt TF-3000) using a triangular AC electric field of ± 200 kV cm^{-1} amplitude with a frequency of 1 kHz. The wake-up behavior, which will be explained in the ferroelectric properties section, was measured using a rectangular AC field of ± 200 kV cm^{-1} amplitude with a frequency of 10 Hz to cycle the samples 10^4 times.

■ RESULTS AND DISCUSSION

Microstructure of PZT and LNO. The first investigated parameter is the oxygen pressure (set A) during the LNO deposition. The samples at various oxygen pressures were investigated by means of AFM and SEM analysis. Figure 1a−d shows the surface topography (top-row AFM) and micro-structure change in the cross section of the PZT (bottom row SEM) while increasing the O$_2$ pressure from 0.1 to 0.8 mbar. The AFM images show that relatively smooth, wide areas are visible at low O$_2$ pressures, and the roughness in these wide areas increases with increasing O$_2$ pressure. Boundaries that are more than 200 nm high in between the wide areas correspond to the gaps in between the individual nanosheet flakes where the PZT exhibits (110)-oriented growth with a faster growth rate than for the (001) orientation.[30] In the following section, we compare only the changes that occur on top of the CNO nanosheet-coated areas covering over 95% of the sample, neglecting the gap areas. The RMS roughness in the CNO nanosheet-coated areas increases 3-fold (7.2 to 23.4 nm) with increasing O$_2$ pressure (Table 1). The cross-sectional SEMs show that with increasing oxygen pressure, the PZT starts to become more columnar and the columnar microstructure

becomes visible earlier in the growth direction of the PZT film. For low O$_2$ pressure, the columns are present only at the top 50 to 100 nm of the PZT film, whereas for the highest O$_2$ pressure, the PZT film grows in columns after half of the thickness is achieved and the top ~500 nm is columnar. Overall, the trend toward columnar microstructure with increasing O$_2$ pressures is evident. On the other hand, this parameter scan does not give any idea if the total pressure, or the O$_2$ partial pressure (p.p.), is playing the dominant role in the microstructural change. For clarification, in set B the total pressure is kept at 0.8 mbar, the same as the highest oxygen pressure in set A, while the oxygen and argon partial pressures are set to 0.1 and 0.7 mbar, respectively. This set allows us to distinguish the influences of the pressure of the O$_2$, which can chemically interact with the deposited film, and the inert Ar. The results in Figure 1e show that the sample surface is a factor of 2 less rough than for sample A4 deposited at 0.8 mbar O$_2$ pressure (Table 1). The cross-sectional SEM also shows that the bulk of the PZT film is dense and that only the top part shows a few columns similar to those of the low-O$_2$-pressure depositions.

The next parameter that was investigated was the thickness of the LNO layer. The LNO layer thickness was increased by ~2.5 times in set C for 0.1 and 0.5 mbar O$_2$ pressures. We compared samples A1 to C1 (Figure 1a−f) and samples A3 to C2 (Figure 1c−g). At low O$_2$ pressure (0.1 mbar), increasing the thickness results in a 3 times rougher PZT film surface: the RMS roughness increases from 7.2 to 24.9 nm. This increase in roughness is due to the change in PZT microstructure from a completely dense, smooth film to a film that grows in separated columns in the top third part of its total thickness. The comparison of the effect of thickness at an O$_2$ pressure of 0.5 mbar shows the same trend but with a less drastic change. The RMS roughness increases from only 20.3 to 26.3 nm. This can
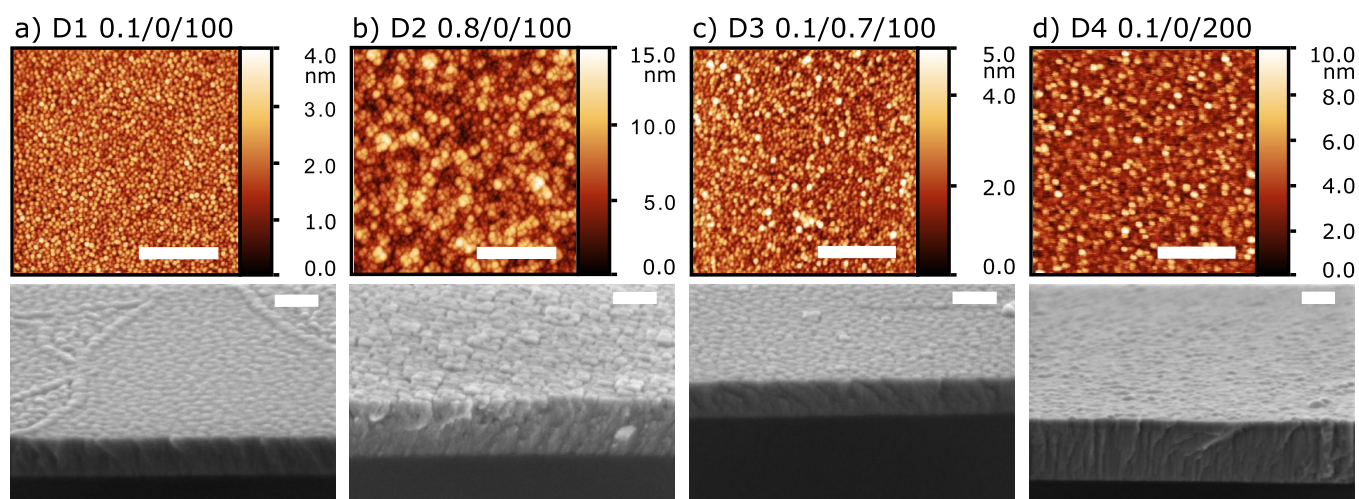
Figure 2. (a−d) AFM surface scans and SEM cross sections for LNO samples. The deposition conditions are given at the top of each panel with the coding sample ID: O2 p.p./Ar p.p./LNO thickness (nm). The scale bar in the SEM corresponds to 100 nm, and that in the AFM, to 500 nm (1.5×1.5 μm^2 area).

be expected if one considers that the PZT surface roughness should reach saturation when the top of the film grows in fully separated columns, and all of the columns have the same diameter and tip shape. The last observation from Figure 1 and Table 1 is the thickness difference between the deposited PZT films, even though their deposition conditions are the same. The more columnar the film, the greater the thickness. This can be explained by considering the stacking of material in the PZT films. The amount of deposited material is the same, but because of the voids between the columns, more material is preferentially stacked in the growth direction on top of the columns.

Until now, we have analyzed the PZT layer to identify the effect of deposition conditions of the template layer. To better investigate the template layer itself, we deposited and analyzed the template layer in set D without adding the PZT layer. To minimize the number of needed samples, only the two extremes of the O_2 pressure (0.1 and 0.8 mbar) (D1 and D2), the deposition at 0.7 mbar p.p. Ar plus 0.1 mbar p.p. O_2 pressure (D3), and the deposition at 0.1 mbar O_2 pressure with a doubled LNO thickness (D4) were investigated. Low O_2 pressure deposition for sample D1, as shown in Figure 2a, has a very smooth LNO surface with the lowest RMS roughness, 0.5 nm. The area scanned with AFM in this set is much smaller than the set A−C samples, spanning only a single nanosheet flake, and hence gap regions are not visible. The SEM cross section shows that the LNO grows mostly dense with round grains visible only at the surface. The sample grown at 0.8 mbar O_2 pressure (D2) has an increased surface RMS roughness of 2.3 nm. The SEM cross section (Figure 2b) shows that the LNO grows less dense and is constituted of columnar LNO grains. The sample grown with 0.1 mbar O_2 p.p. and 0.8 mbar total pressure (D3, shown in Figure 2d) has a surface roughness of 0.8 nm, which is slightly increased in comparison to the surface roughness of the 0.1 mbar sample (D1 in Figure 2a). These two samples show no clear difference in microstructure as seen in the SEM images. Increasing the LNO thickness to 190 nm at 0.1 mbar O_2 pressure (D4) increases the surface roughness by a factor 3 (cf. Figure 2a,d). The cross-sectional SEMs show that the grain size of the LNO is increased for the thicker LNO.

We explain the increasing trend in the columnar PZT microstructure in Figure 1 by the increase in roughness of the template LNO layer due to an increase in either the deposition pressure or the thickness of the LNO layer. This roughness increase leads to a reduced diffusion distance of the deposited PZT and results in columnar growth. According to the literature, the diffusion time for the PZT is low at a high deposition frequency of 50 Hz, and hence columnar growth is promoted.[38] However, in contrast to the literature, we also obtained noncolumnar, dense, smooth films under the literature's deposition conditions, including the 50 Hz deposition frequency of PZT.[38] Our results show that in addition to the high laser repetition frequency, the roughness of the template also plays a crucial role. In the literature, there is also disagreement between experimental findings[38] and theoretical predictions[38,53] regarding the influence of the deposition frequency in PLD. Experiments show very clearly that the PZT grows more columnar at higher repetition frequencies.[38] The theoretical study, which assumes the independence of the growth mode from the deposited material, predicts that the material should grow in a smooth film at high deposition frequencies because of the reduced size of the nucleating islands and the enhanced diffusion of adatoms from the top of the growing islands to the substrate.[53] Our observation of a dense film at the high deposition frequency can help to solve the disagreement in these findings. If the growth template is smooth, then the grown film is smooth as theoretically predicted,[53] whereas in the case of a rough template, the diffusion of adatoms does not take place and the material starts to grow in separated columns, especially at higher frequencies.

Another finding based on set B was that not the total pressure but the oxygen partial pressure is the deciding factor in determining the roughness and microstructure of the LNO layer. The microstructure of B1, with the 0.1 mbar O_2 p.p. and 0.8 mbar total pressure, is more comparable to that of a sample grown at 0.25 mbar O_2 pressure but not to the sample grown at 0.8 mbar O_2 pressure. This observation points out that the dominant parameter is not the kinetic energy of the ablated material but the interaction of the ablated species with the reactive O_2 gas. For higher oxygen pressure, the ablated material seems to interact more with the oxygen and form
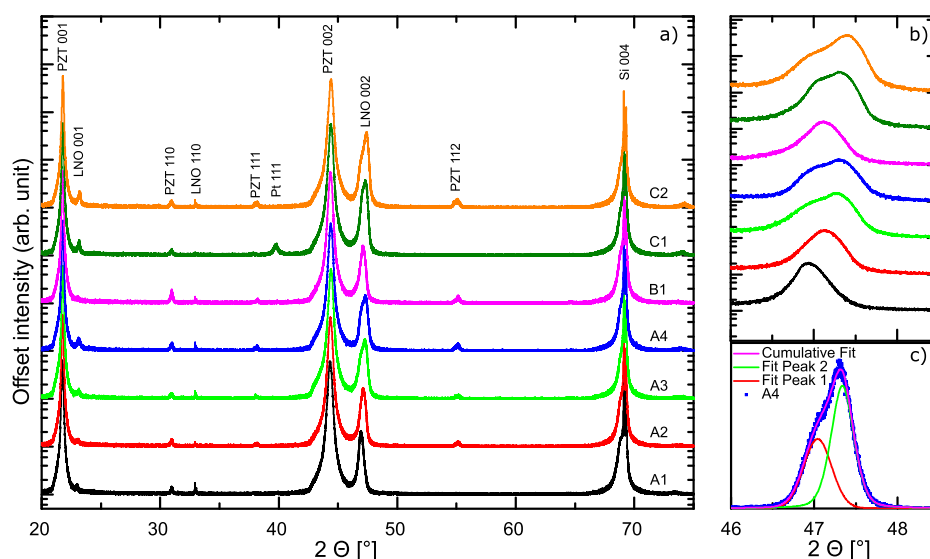
Figure 3. (a) XRD survey spectra of the LNO\PZT samples. (b) Detailed view of the LNO(002) peaks. (c) Fitting of the LNO(002) peaks of sample A4 with two Voight functions.

Table 2. Peak Position, Width (fwhm), Area, and Area Ratio of the Fitted Voight Functions for all LNO\PZT Samples

	peak 1			peak 2			
sample	position	fwhm	area	position	fwhm	area	area(peak 2)/area(peak 1)
A1	46.95	0.31	750	47.14	0	0	0.0 ± 0
A2	47.06	0.31	468	47.22	0.25	184	0.39 ± 0.03
A3	47.06	0.26	457	47.31	0.30	371	0.81 ± 0.21
A4	47.04	0.39	270	47.34	0.32	426	1.6 ± 0.15
B1	47.05	0.29	469	47.20	0.23	157	0.33 ± 0.02
C1	47.09	0.33	699	47.32	0.30	1008	1.4 ± 0.27
C2	47.00	0.36	459	47.38	0.33	1238	2.7 ± 0.20

clusters of multiple unit cells in the plasma plume.[54] If these clusters are deposited on the substrate, we do not have the unit-cell by unit-cell buildup known from epitaxial films but a cluster-by-cluster growth. These clusters have a lower mobility and form rough islands as seeds for further columnar growth.

Crystal Structure. The out-of-plane crystal orientations of the PZT samples, sets A−C, were characterized by XRD θ−2θ scans as shown in Figure 3a. Both PZT and LNO grow mainly with (001) orientation with small (110) and (111) peaks. According to the literature, the (110) and (111) peaks can be attributed to the growth in the gap regions between the nanosheets, directly on the Si substrate.[38,39,55] The Pt(111) peak in sample C1 is due to the measurement of the sample only after the top Pt electrode structuring. The changes in the deposition conditions of the LNO template do not seem to visibly influence the crystallinity of the atop-grown PZT. The LNO(002) peaks show some changes with the deposition conditions, as more clearly visible in Figure 3b. One observes that the LNO(002) peak has a broad, double-peak structure and is shifted to higher angles for increasing oxygen pressure and higher LNO film thickness. The 2θ angles of the individual peaks in this double-peak structure are around the in-plane lattice parameters of CNO (47.088°)[26,27] and the bulk pseudocubic lattice parameter of LNO (47.348°).[37,56] Describing our LNO film with a pseudocubic lattice of equal in-plane and out-of-plane lattice parameters, these double peaks point to two crystal structures with two different in- and out-of-plane lattice parameters. It is conceivable that the

bottom part of the LNO grows in an epitaxially strained manner to the CNO nanosheet, resulting in the first XRD peak matching the CNO lattice parameter at a lower 2θ angle. The top part of the LNO, however, is relaxed to the bulk lattice parameter of LNO, resulting in the second observed peak at a higher 2θ angle. Therefore, with increasing O_2 pressure and thickness, the LNO is less strained with respect to the CNO nanosheet and relaxes to the bulk LNO lattice parameters.

The observed relaxation with increasing film thickness was reported for an LNO layer that was sputtered directly onto the Si substrate and was attributed to the relaxation of the thermal strain.[56] In another report on the LNO films deposited on LaAlO$_3$ substrates, decreasing O_2 pressure produces less-strained films because of the incorporation of the oxygen vacancies.[57] However, neither of these reports presents a double-peak structure for the LNO but only a shift of the LNO peak. To explain the observed double-peak structures, the relaxation of thermal strain is not sufficient because the thermal strain would be same for the whole LNO film and would not lead to a splitting of the peak. We attribute our observations to epitaxial strain relaxation. For low O_2 pressure and a thickness of about 100 nm, the LNO grows in an epitaxially strained manner to the CNO nanosheet, and further increases in O_2 pressure or thickness lead to a roughening of the film, as observed in sample set D, to release the strain.

To quantify the strained and relaxed fractions of the LNO films, we fitted the (002) peaks of all samples in the 46 to 48.5° range with two Voight functions after subtracting a linear

background. The fitting for sample A4 is shown in Figure 3c as an example. Table 2 gives the central positions, widths (fwhm), areas, and area ratios of the fitted peaks. For all of the samples, the positions of the first and second peaks match the expected 47.088 and 47.348°, respectively, when the 0.15° systematic error bars are taken into account. The large systematic error bars in the peak positions are due to difficulty in the alignment. The samples were aligned with respect to the Si(004) peak. However, the LNO\PZT grows on the nanosheets that are not coupled to the crystal orientation of Si, leading to peak shifts of ±0.15°. In addition to this, the samples with low O_2 pressure (A1, A2, and B1) exhibit larger peak shifts from the bulk values. We attribute these shifts to the numerical inaccuracy of the fits due to the very small size of the second peaks.

Discussion of the Growth Mode. It is clear from the SEM pictures in Figures 1 and 2 and the extracted roughness values in Table 1 that the roughness of the PZT layer is a good indicator of the level of columnarity of the film. Besides the roughness of the PZT, it is instructive to search for quantified indicators in the LNO template layer to better understand and connect the growth mechanism to the template layer. Considering that the epitaxial strain is relaxed by increasing the roughness, we hypothesize that the area ratio of the relaxed to strained part of the LNO layer, area(peak 2)/area(peak 1), can be such an indicator. It is possible then to check the correlation of the PZT surface roughness and the LNO peak-area ratio as plotted in Figure 4. One observes that there is a
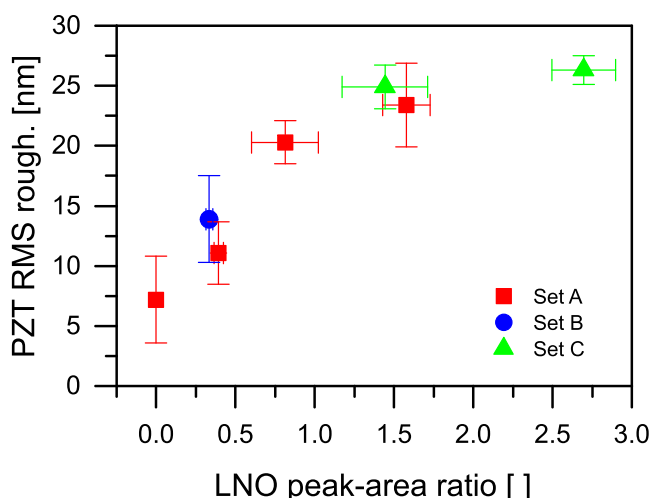

Figure 4. RMS roughness of the PZT against the peak-area ratio of the LNO for all LNO\PZT samples.

high correlation between the peak-area ratio and the PZT surface roughness. For small peak ratios, the RMS roughness is small, showing that the PZT growth is dense. All samples with a peak-area ratio above 0.8 shows a high RMS roughness above 20 nm, where the PZT growth is columnar, as verified by the SEM images.

We propose that for the growth of the samples with a peak-area ratio of below 0.8, the PZT molecules arriving from the target prefer to assemble epitaxially on the LNO via Frank−van der Merwe growth, which is a layer-by-layer growth.[58] For this growth mode, the specific surface free energy of the LNO−vacuum interface has to be larger than that of LNO−PZT and PZT−vacuum interfaces. For the samples with a peak-area ratio above 0.8, the growth of PZT is initially layer-

by-layer growth. However, at a critical thickness, because of the increased roughness originating from the LNO template, the formation of coherent 3D islands is preferred. The 3D island growth significantly reduces the surface energy due to elastic relaxation of the strain field in islands via Volmer−Weber growth.[59] The combination of the starting layer by layer growth with the formation of 3D islands after a certain thickness is referred to as the Stranski−Krastanov growth model.[60] Further arriving PZT molecules preferentially grow on the 3D islands because of energy reduction, leading to well-oriented columnar growth at the top of the film that we observe. The resulting roughness is much higher than layer-by-layer growth and also reaches saturation. The saturation in roughness can be understood by considering that the PZT surface roughness will not increase further if the film growth at the top is completely columnar, and all of the columns have the same diameter and tip shape. The level of saturation occurs above 25 nm for the investigated PZT films, but it may vary for different materials.

Ferroelectric Properties. In the following section, the influence of the deposition conditions of the LNO template layer on the ferroelectric properties of the PZT film is investigated. The literature shows that the electrical properties of LNO films in the range of our deposition pressures and thicknesses do not change significantly.[56,57] Therefore, the observed changes in the ferroelectric properties can be attributed to either the electrode−PZT interfaces or the PZT layer itself. We observed changing ferroelectric properties, especially remnant polarization P_r, with the number of measurement cycles as shown in Figure 5a. The coercive field E_c shows no clear trend, so it is not plotted. Before comparing samples, first we explain the evolution of the remnant polarization. In all samples, the remnant polarization P_r increases first, reaches a maximum of between 10^2 and 10^3 cycles, and then decreases. Only sample C1 exhibits different behavior with a sharp decrease after 158 cycles because of the electrical breakdown of the sample. The sample breakdown is due to the longer storage of the sample in air (3 months) compared to that of the other samples that were measured shortly after the fabrication. It is known that air humidity causes the degradation of the Pt top electrodes on PZT films, leading to an earlier electrical breakdown.[61] Nevertheless, until the breakdown the sample behavior is similar to that of samples A3 and A4, as expected from Figure 4.

To investigate the changes in the ferroelectric properties with cycling in more detail, the sample that shows the most apparent evolution, sample A1, is used as an example. The P−E and I−E loops are shown in Figure 5b,c for three different cycling states. The initial loop before cycling is applied, along with the loop at the highest remnant polarization which occurs after 1.58×10^2 cycles and the loop after the maximum number of 10^4 cycles. The P−E loops show squarelike behavior, indicating good ferroelectric quality. We observe that all loops are slightly slanted and asymmetric around the horizontal axis. The slantedness of the loop decreases as the number of cycles increases from 1 to 1.58×10^2, and thus the remnant polarization P_r is increasing and reaches a maximum at 1.58×10^2 cycles. Afterward, P_r decreases continuously with an increasing number of cycles. The asymmetry of the P−E loop is attributed to the difference in the work function of the electrodes that are from two different materials, namely, LNO and Pt.[21,62] The changes due to cycling are even more clearly visible in the I−E loops. With an increasing number of cycles,
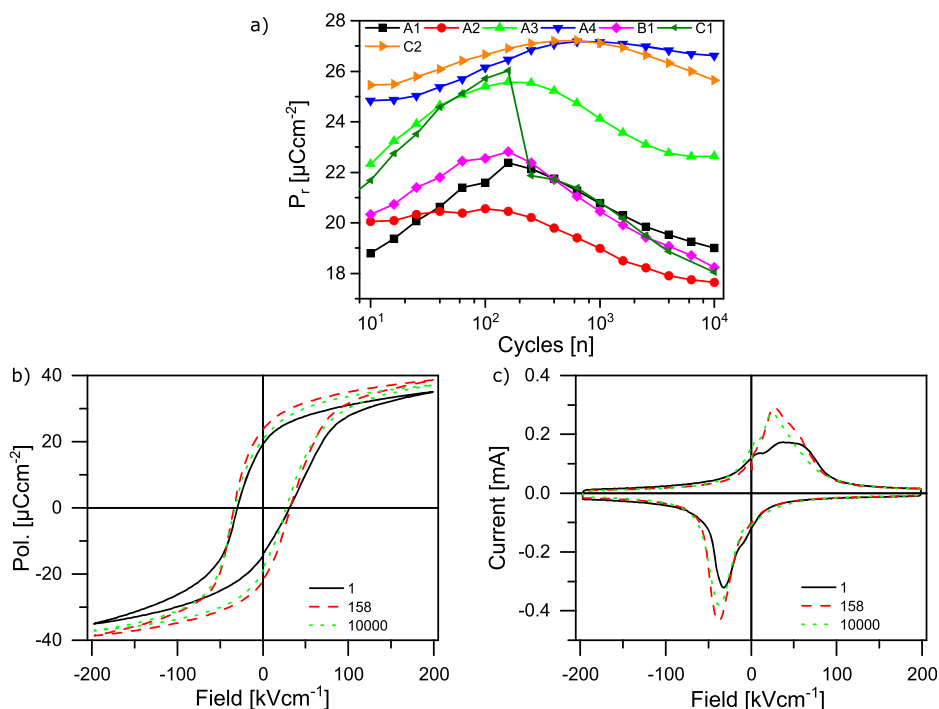
Figure 5. (a) Effect of electric-field cycling on the remnant polarization P_r for all samples with LNO\PZT. Sample C1 shows a sharp decrease after 158 cycles due to an electrical breakdown; see the main text. (b) P−E loop and (c) I−E loop for sample A1 with an increasing number of electrical field cycles.
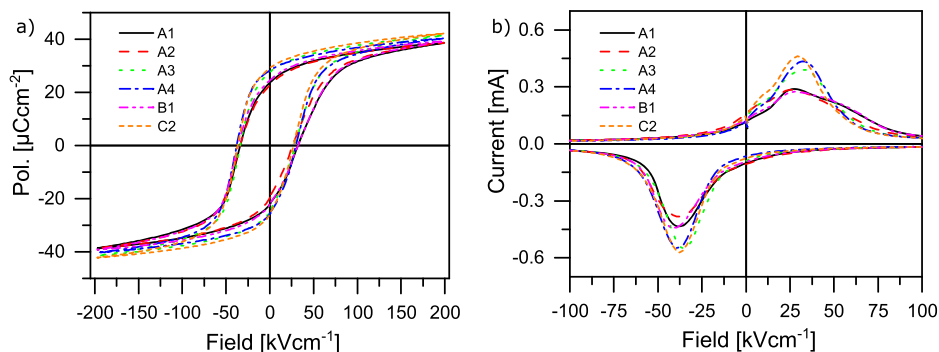

Figure 6. (a) P−E and (b) I−E loops in the awake state where the maximum P_r is observed for sample sets A−C. For better visibility, only the data between ±100 kV/cm is shown for the I−E loops. The difference between the samples outside this range was negligibly small.

the broad initial peak narrows on both sides and a sharp peak develops. After 1.58×10^2 cycles, the peak value starts to decrease but the shape is mostly preserved, with slight slimming. The negative switching peaks exhibit similar behavior with an increasing number of cycles.

The increase in P_r with cycling is known as a wake-up effect and is reported for some PZT films[63] and more commonly for HfO$_2$-based ferroelectrics.[64−68] The wake up for PZT is mostly observed for sol−gel films and is attributed to the pinning of domains in the films, which leads to internal bias fields and double peaks in the I−E loops.[65] With increased cycling of the electric field, the domains that are pinned because of defects such as point defects, oxygen and/or lead vacancies, and grain boundaries reorient themselves.[65,69−73] The thus-formed new domain structure is more stable and has a higher remnant polarization. The absence of two clearly visible switching peaks in our films can be explained by the higher film quality due to PLD growth compared to sol−gels. Because of the better film quality, we have fewer defects and thus the domains are only

slightly pinned and do not form the clear double-peak structure. Comparing the amount of wake up between our samples, the differences can be correlated with the microstructure. For the columnar PZT samples, the grain size is smaller and the domains are less clamped and as a result are easier to switch and reach a stable domain configuration. The decrease in P_r with further increases in the number of cycles, i.e. fatigue, is well known for samples with Pt electrodes.[74] It is explained mainly by two models. The first model explains the polarization decrease with the migration and accumulation of oxygen vacancies at the film−electrode interface, causing domain pinning and charge screening.[75−80] The second model considers the interfacial layer injecting electrons into the ferroelectric layer, leading to decomposition of the ferroelectric layer.[81−84] The existence of such an interfacial layer in the PLD PZT films has recently been proven using TEM measurements.[85]

To make a fair comparison of the influence of the template layer on the ferroelectric properties, we compare the P−E and

I—E loops of all samples after wake-up, so where P_r is maximized in Figure 6. Because sample C1 broke before reaching the maximum, it is excluded from Figure 6. In the P—E loops, the differences in the P_r and maximum polarization P_{max} are visible, but changes in the coercive fields are less visible. For the samples with an RMS roughness of >20 nm and an LNO peak/area ratio of >0.8 (A3, A4, and C2), the slantedness of the P—E loops decreases, which results in increases in P_r and P_{max}. The P_{max} values measured for these samples are similar to the values reported on PZT films of the same thickness deposited on 100-nm-thick $SrRuO_3$ electrodes on Si\CNO substrates[30] and PZT films of 750 nm thickness grown on 200-nm-thick LNO on glass\CNO substrates[27] but smaller than values reported for films grown epitaxially on STO.[30] The samples with an RMS roughness of <20 nm and an LNO peak/area ratio of <0.8 (A1, A2, and B1) have a lower P_{max} and P_r that are comparable with the structures deposited on Si\Pt\CNO substrates.[30] The samples with high roughness (>20 nm) have on average 1.2 times higher remnant polarizations than the samples with low roughness, underlining the influence of the microstructure on the ferroelectric properties. In the I—E loops, the positive switching peaks are broader than the negative switching peaks for all samples as a result of the difference in the top and bottom electrode materials. The literature attributes wider switching peaks to larger variations in the grain size.[86] This literature finding suggests that the grain size variation is largest for the densest PZT films. Our films are consistent with this literature suggestion, considering that the grains in our dense PZT films can grow laterally as large as the few-micrometer-sized CNO nanosheets with a wide size distribution.[55] On the other hand, for the columnar films the column diameters are similar (between 100 and 150 nm) and about a factor of 10 smaller than a micrometer. The grain size distribution is no longer dependent on the size of the nanosheet. Correspondingly, these samples have sharper switching peaks.

Within this study, we observe a clear correlation between the film microstructure and remnant polarization P_r. The maximum polarization, however, does not clearly corollate with the film microstructure because its value is not increasing continuously with increasing roughness. Thus, for energy storage devices, it is important to take the effect of the microstructure on the ferroelectric properties into account when aiming to improve the energy storage capacities. The increases in the ferroelectric properties with increased roughness can be a clear indication of an increase in the piezoelectric properties through electrostriction.[87] The longitudinal piezoelectric coefficient $d_{33,f}$ is proportional to P^2, so $d_{33,f}$ is expected to be higher for the rougher films with columnar microstructure. This effect has been shown by the work of Nguyen et al., who have investigated the effect of the deposition conditions of the PZT on the film properties.[30,38−40] These works clearly show that the growth of columnar PZT leads to a reduction of the clamping effect, thus reducing the d_{31} coefficient and increasing the $d_{33,f}$ coefficient for columnar films. The ability to control the film microstructure using the template layer, from a dense, smooth PZT film to a rough, columnar PZT film, is interesting for actuators because this allows control of the preferred actuation mode between the d_{31} mode with dense films or the $d_{33,f}$ mode with columnar films.

■ CONCLUSIONS

We demonstrated the influence of the deposition pressure and the thickness of the LNO template layer on the microstructure and the ferroelectric properties of the subsequently grown PZT film. A higher oxygen pressure and a greater thickness of the LNO template were found to lead to a higher roughness and the columnar growth of the PZT film. We attribute the change in the growth from 2D layer-by-layer growth to 3D island growth to the increased roughness of the LNO layer in order to relax the epitaxial strain. The ferroelectric properties of the PZT films are improved for the films with columnar microstructure. This increase is explained by the reduced lateral grain size of the columnar PZT films. The average lateral grain size is much smaller and is determined by the column width in columnar films, in contrast to the grain sizes that can reach the lateral size of a micrometer-sized nanosheet in dense films. The columnar microstructure leads to a smaller and more even grain size distribution and thus to changed ferroelectric properties.

■ AUTHOR INFORMATION

Corresponding Author

Philip Lucke − *Industrial Focus Group XUV Optics, MESA+ Institute for Nanotechnology, Universiteit Twente, Enschede, Overijssel 7500 AE, The Netherlands;* orcid.org/0000-0003-3636-6138; Email: p.lucke@utwente.nl

Authors

Mohammadreza Nematollahi − *Industrial Focus Group XUV Optics, MESA+ Institute for Nanotechnology, Universiteit Twente, Enschede, Overijssel 7500 AE, The Netherlands;* Present Address: Radboud University Nijmegen, Trace Gas Research Group, Department of Molecular and Laser Physics, Institute of Molecules and Materials, P.O. Box 9010 Nijmegen, Gelderland, The Netherlands 6500 HC

Muharrem Bayraktar − *Industrial Focus Group XUV Optics, MESA+ Institute for Nanotechnology, Universiteit Twente, Enschede, Overijssel 7500 AE, The Netherlands*

Andrey E. Yakshin − *Industrial Focus Group XUV Optics, MESA+ Institute for Nanotechnology, Universiteit Twente, Enschede, Overijssel 7500 AE, The Netherlands*

Johan E. ten Elshof − *Inorganic Material Science, MESA+ Institute for Nanotechnology, Universiteit Twente, Enschede, Overijssel 7500 AE, The Netherlands;* orcid.org/0000-0001-7995-6571

Fred Bijkerk − *Industrial Focus Group XUV Optics, MESA+ Institute for Nanotechnology, Universiteit Twente, Enschede, Overijssel 7500 AE, The Netherlands*

Complete contact information is available at:
https://pubs.acs.org/10.1021/acsomega.2c00815

■ ACKNOWLEDGMENTS

■ REFERENCES

(1) Nagarajan, V.; Stanishevsky, A.; Chen, L.; Zhao, T.; Liu, B.-T.; Melngailis, J.; Roytburd, A. L.; Ramesh, R.; Finder, J.; Yu, Z.; et al. Realizing intrinsic piezoresponse in epitaxial submicron lead zirconate titanate capacitors on Si. *Appl. Phys. Lett.* **2002**, *81* (22), 4215−4217.

(2) Trolier-McKinstry, S.; Muralt, P. Thin Film Piezoelectrics for MEMS. *J. Electroceram.* **2004**, *12* (1), 7−17.

(3) Setter, N.; Damjanovic, D.; Eng, L.; Fox, G.; Gevorgian, S.; Hong, S.; Kingon, A.; Kohlstedt, H.; Park, N. Y.; Stephenson, G. B.; et al. Ferroelectric thin films: Review of materials, properties, and applications. *J. Appl. Phys.* **2006**, *100* (5), 051606.

(4) Eom, C.-B.; Trolier-McKinstry, S. Thin-film piezoelectric MEMS. *MRS Bull.* **2012**, *37* (11), 1007−1017.

(5) Smith, G. L.; Pulskamp, J. S.; Sanchez, L. M.; Potrepka, D. M.; Proie, R. M.; Ivanov, T. G.; Rudy, R. Q.; Nothwang, W. D.; Bedair, S. S.; Meyer, C. D.; et al. PZT-Based Piezoelectric MEMS Technology. *J. Am. Ceram. Soc.* **2012**, *95* (6), 1777−1792.

(6) Bayraktar, M.; Wessels, W. A.; Lee, C. J.; van Goor, F. A.; Koster, G.; Rijnders, G.; Bijkerk, F. Active multilayer mirrors for reflectance tuning at extreme ultraviolet (EUV) wavelengths. *J. Phys. D: Appl. Phys.* **2012**, *45* (49), 494001.

(7) Bayraktar, M.; Chopra, A.; Rijnders, G.; Boller, K.; Bijkerk, F. Wavefront correction in the extreme ultraviolet wavelength range using piezoelectric thin films. *Opt. Express* **2014**, *22* (25), 30623−30632.

(8) Nematollahi, M.; Lucke, P.; Bayraktar, M.; Yakshin, A.; Rijnders, G.; Bijkerk, F. Nanoscale piezoelectric surface modulation for adaptive extreme ultraviolet and soft x-ray optics. *Opt. Lett.* **2019**, *44* (20), 5104−5107.

(9) Khan, M. B.; Kim, D. H.; Han, J. H.; Saif, H.; Lee, H.; Lee, Y.; Kim, M.; Jang, E.; Hong, S. K.; Joe, D. J.; et al. Performance improvement of flexible piezoelectric energy harvester for irregular human motion with energy extraction enhancement circuit. *Nano Energy* **2019**, *58*, 211−219.

(10) Han, J. H.; Park, K.-I.; Jeong, C. K. Dual-Structured Flexible Piezoelectric Film Energy Harvesters for Effectively Integrated Performance. *Sensors* **2019**, *19* (6), 1444.

(11) Jaffe, B.; Cook, W. R.; Jaffe, H. In *Piezoelectric Ceramics*; Jaffe, B., Cook, W. R., Jaffe, H., Eds.; Academic Press, 1971; Chapter 7, pp 135−183.

(12) Haun, M. J.; Furman, E.; Jang, S. J.; Cross, L. E. Thermodynamic theory of the lead zirconate-titanate solid solution system, part V: Theoretical calculations. *Ferroelectrics* **1989**, *99* (1), 63−86.

(13) Guo, R.; Cross, L. E.; Park, S. E.; Noheda, B.; Cox, D. E.; Shirane, G. Origin of the High Piezoelectric Response in PbZr1-xTixO3. *Phys. Rev. Lett.* **2000**, *84* (23), 5423−5426.

(14) Damjanovic, D. A morphotropic phase boundary system based on polarization rotation and polarization extension. *Appl. Phys. Lett.* **2010**, *97* (6), 062906.

(15) Du, X.-h.; Belegundu, U.; Uchino, K. Crystal Orientation Dependence of Piezoelectric Properties in Lead Zirconate Titanate: Theoretical Expectation for Thin Films. *Jpn. J. Appl. Phys.* **1997**, *36* (Part 1, No. 9A), 5580−5587.

(16) Ouyang, J.; Yang, S. Y.; Chen, L.; Ramesh, R.; Roytburd, A. L. Orientation dependence of the converse piezoelectric constantsfor epitaxial single domain ferroelectric films. *Appl. Phys. Lett.* **2004**, *85* (2), 278−280.

(17) Kim, C. J.; Yoon, D. S.; Lee, J. S.; Choi, C. G.; Lee, W. J.; No, K. Electrical characteristics of (100), (111), and randomly aligned lead zirconate titanate thin films. *J. Appl. Phys.* **1994**, *76* (11), 7478−7482.

(18) Du, X.-h.; Zheng, J.; Belegundu, U.; Uchino, K. Crystal orientation dependence of piezoelectric properties of lead zirconate titanate near the morphotropic phase boundary. *Appl. Phys. Lett.* **1998**, *72* (19), 2421−2423.

(19) Muralt, P. Ferroelectric thin films for micro-sensors and actuators: a review. *J. Micromech. Microeng.* **2000**, *10* (2), 136−146.

(20) Bao, D.; Scholz, R.; Alexe, M.; Hesse, D. Growth, microstructure, and ferroelectric properties of Pb(Zr0.4Ti0.6)O3/PbZrO3 superlattices prepared on SrTiO3 (100) substrates by pulsed laser deposition. *J. Appl. Phys.* **2007**, *101* (5), 054118.

(21) Baek, S. H.; Park, J.; Kim, D. M.; Aksyuk, V. A.; Das, R. R.; Bu, S. D.; Felker, D. A.; Lettieri, J.; Vaithyanathan, V.; Bharadwaja, S. S. N.; et al. Giant Piezoelectricity on Si for Hyperactive MEMS. *Science* **2011**, *334* (6058), 958−961.

(22) Fork, D. K.; Fenner, D. B.; Connell, G. A. N.; Phillips, J. M.; Geballe, T. H. Epitaxial yttria-stabilized zirconia on hydrogen-terminated Si by pulsed laser deposition. *Appl. Phys. Lett.* **1990**, *57* (11), 1137−1139.

(23) Kumar, A.; Alam, M. R.; Mangiaracina, A.; Shamsuzzoha, M. Synthesis of the PZT films deposited on pt-coated (100) Si substrates for nonvolatile memory applications. *J. Electron. Mater.* **1997**, *26* (11), 1331−1334.

(24) Wang, S. J.; Ong, C. K.; You, L. P.; Xu, S. Y. Epitaxial growth of yittria-stabilized zirconia oxide thin film on natively oxidized silicon wafer without an amorphous layer. *Semicond. Sci. Technol.* **2000**, *15* (8), 836−839.

(25) Dekkers, M.; Nguyen, M. D.; Steenwelle, R.; Riele, P. M. t.; Blank, D. H. A.; Rijnders, G. Ferroelectric properties of epitaxial Pb(Zr,Ti)O3 thin films on silicon by control of crystal orientation. *Appl. Phys. Lett.* **2009**, *95* (1), 012902.

(26) Kikuta, K.; Noda, K.; Okumura, S.; Yamaguchi, T.; Hirano, S.-i. Orientation control of perovskite thin films on glass substrates by the application of a seed layer prepared from oxide nanosheets. *J. Sol-Gel Sci. Technol.* **2007**, *42* (3), 381−387.

(27) Bayraktar, M.; Chopra, A.; Bijkerk, F.; Rijnders, G. Nanosheet controlled epitaxial growth of PbZr0.52Ti0.48O3 thin films on glass substrates. *Appl. Phys. Lett.* **2014**, *105* (13), 132904.

(28) Minemura, Y.; Kondoh, Y.; Funakubo, H.; Uchida, H. One-Axis-Oriented Crystal Growth of Lead Zirconate Titanate Thin Films on Metal Substrates Using Perovskite-Type Oxide Nanosheet Layer. *Key Eng. Mater.* **2013**, *582*, 15−18.

(29) Chopra, A.; Bayraktar, M.; Bijkerk, F.; Rijnders, G. Controlled growth of PbZr0.52Ti0.48O3 using nanosheet coated Si (001). *Thin Solid Films* **2015**, *589*, 13−16.

(30) Nguyen, M. D.; Yuan, H.; Houwman, E. P.; Dekkers, M.; Koster, G.; ten Elshof, J. E.; Rijnders, G. Highly Oriented Growth of Piezoelectric Thin Films on Silicon Using Two-Dimensional Nanosheets as Growth Template Layer. *ACS Appl. Mater. Interfaces* **2016**, *8* (45), 31120−31127.

(31) Uchida, H.; Ichinose, D.; Shiraishi, T.; Shima, H.; Kiguchi, T.; Akama, A.; Nishida, K.; Konno, T. J.; Funakubo, H. Polarization switching behavior of one-axis-oriented lead zirconate titanate films fabricated on metal oxide nanosheet layer. *Jpn. J. Appl. Phys.* **2017**, *56* (10S), 10PF10.

(32) Izyumskaya, N.; Alivov, Y. I.; Cho, S. J.; Morkoç, H.; Lee, H.; Kang, Y. S. Processing, structure, properties, and applications of PZT thin films. *Crit. Rev. Solid State Mater. Sci.* **2007**, *32* (3−4), 111−202.

(33) Houwman, E. P.; Nguyen, M. D.; Dekkers, M.; Rijnders, G. Intrinsic stability of ferroelectric and piezoelectric properties of epitaxial PbZr 0.45 Ti 0.55 O 3 thin films on silicon in relation to grain tilt. *Sci. Technol. Adv. Mater.* **2013**, *14* (4), 045006.

(34) Ganpule, C. S.; Stanishevsky, A.; Aggarwal, S.; Melngailis, J.; Williams, E.; Ramesh, R.; Joshi, V.; Araujo, C. P. d. Scaling of

ferroelectric and piezoelectric properties in Pt/SrBi2Ta2O9/Pt thin films. *Appl. Phys. Lett.* **1999**, 75 (24), 3874−3876.

(35) Bühlmann, S.; Dwir, B.; Baborowski, J.; Muralt, P. Size effect in mesoscopic epitaxial ferroelectric structures: Increase of piezoelectric response with decreasing feature size. *Appl. Phys. Lett.* **2002**, 80 (17), 3195−3197.

(36) Li, J.-H.; Chen, L.; Nagarajan, V.; Ramesh, R.; Roytburd, A. L. Finite element modeling of piezoresponse in nanostructured ferroelectric films. *Appl. Phys. Lett.* **2004**, 84 (14), 2626−2628.

(37) Chopra, A.; Bayraktar, M.; Nijland, M.; ten Elshof, J. E.; Bijkerk, F.; Rijnders, G. Tuning of large piezoelectric response in nanosheet-buffered lead zirconate titanate films on glass substrates. *Sci. Rep.* **2017**, 7, 251.

(38) Nguyen, M. D.; Houwman, E. P.; Yuan, H.; Wylie-Van Eerd, B. J.; Dekkers, M.; Koster, G.; Ten Elshof, J. E.; Rijnders, G. Controlling Piezoelectric Responses in Pb(Zr0.52Ti0.48)O3 Films through Deposition Conditions and Nanosheet Buffer Layers on Glass. *ACS Appl. Mater. Interfaces* **2017**, 9 (41), 35947−35957.

(39) Nguyen, M. D.; Houwman, E. P.; Rijnders, G. Large piezoelectric strain with ultra-low strain hysteresis in highly c-axis oriented Pb(Zr0.52Ti0.48)O3 films with columnar growth on amorphous glass substrates. *Sci. Rep.* **2017**, 7 (1), 12915.

(40) Nguyen, M. D.; Houwman, E. P.; Dekkers, M.; Rijnders, G. Strongly Enhanced Piezoelectric Response in Lead Zirconate Titanate Films with Vertically Aligned Columnar Grains. *ACS Appl. Mater. Interfaces* **2017**, 9 (11), 9849−9861.

(41) Chu, F.; Xu, F.; Shepard, J.; Trolier-McKinstry, S. Thickness Dependence of the Electrical Properties of Sol-Gel Derived Lead Zirconate Titanate Thin Films with (111) and (100) Texture. *MRS Proceedings* **1997**, 493, 409.

(42) Tang, X. G.; Chan, H. L. W.; Ding, A. L.; Yin, Q. Processing effects on the microstructure and ferroelectric properties of Pb(Zr,Ti)O3 thin films prepared by sol−gel process. *Surf. Coat. Technol.* **2002**, 161 (2), 169−173.

(43) Bouregba, R.; Poullain, G.; Vilquin, B.; Murray, H. Epitaxial PZT thin films on TiOx covered Pt/MgO substrate by RF magnetron sputtering. *Ferroelectrics* **2001**, 256 (1), 47−68.

(44) Kanno, I.; Kotera, H.; Wasa, K.; Matsunaga, T.; Kamada, T.; Takayama, R. Crystallographic characterization of epitaxial Pb(Zr,Ti)-O3 films with different Zr/Ti ratio grown by radio-frequency-magnetron sputtering. *J. Appl. Phys.* **2003**, 93 (7), 4091−4096.

(45) Jacobsen, H.; Prume, K.; Wagner, B.; Ortner, K.; Jung, T. High-rate sputtering of thick PZT thin films for MEMS. *J. Electroceram.* **2010**, 25 (2), 198−202.

(46) Nordseth, Ø.; You, C. C.; Folven, E.; Gariglio, S.; Sambri, A.; Triscone, J.-M.; Reiner, J. W.; Ahn, C. H.; Tybell, T.; Grepstad, J. K. Growth and characterization of (Pb,La)(Zr,Ti)O3 thin film epilayers on SrTiO3-buffered Si(001). *Thin Solid Films* **2010**, 518 (19), 5471−5477.

(47) Yoshida, S.; Hanzawa, H.; Wasa, K.; Esashi, M.; Tanaka, S. Highly c-axis-oriented monocrystalline Pb(Zr, Ti)O3 thin films on si wafer prepared by fast cooling immediately after sputter deposition. *IEEE Trans. Sonics Ultrason.* **2014**, 61 (9), 1552−1558.

(48) Palneedi, H.; Peddigari, M.; Hwang, G.-T.; Jeong, D.-Y.; Ryu, J. High-Performance Dielectric Ceramic Films for Energy Storage Capacitors: Progress and Outlook. *Adv. Funct. Mater.* **2018**, 28 (42), 1803665.

(49) Liu, H.; Zhong, J.; Lee, C.; Lee, S.-W.; Lin, L. A comprehensive review on piezoelectric energy harvesting technology: Materials, mechanisms, and applications. *Appl. Phys. Rev.* **2018**, 5 (4), 041306.

(50) Sarker, M. R.; Julai, S.; Sabri, M. F. M.; Said, S. M.; Islam, M. M.; Tahir, M. Review of piezoelectric energy harvesting system and application of optimization techniques to enhance the performance of the harvesting system. *Sensors and Actuators A: Physical* **2019**, 300, 111634.

(51) Muralt, P.; Polcawich, R. G.; Trolier-McKinstry, S. Piezoelectric Thin Films for Sensors, Actuators, and Energy Harvesting. *MRS Bull.* **2009**, 34 (9), 658−664.

(52) Yuan, H.; Lubbers, R.; Besselink, R.; Nijland, M.; ten Elshof, J. E. Improved Langmuir−Blodgett Titanate Films via in Situ Exfoliation Study and Optimization of Deposition Parameters. *ACS Appl. Mater. Interfaces* **2014**, 6 (11), 8567−8574.

(53) Guan, L.; Zhang, D.; Li, X.; Li, Z. Role of pulse repetition rate in film growth of pulsed laser deposition. *Nucl. Instrum. Methods Phys. Res., Sect. B* **2008**, 266 (1), 57−62.

(54) Chen, Y.-Z.; Liu, T.-H.; Chen, C.-Y.; Liu, C.-H.; Chen, S.-Y.; Wu, W.-W.; Wang, Z. L.; He, J.-H.; Chu, Y.-H.; Chueh, Y.-L. Taper PbZr0.2Ti0.8O3 Nanowire Arrays: From Controlled Growth by Pulsed Laser Deposition to Piezopotential Measurements. *ACS Nano* **2012**, 6 (3), 2826−2832.

(55) Yuan, H.; Nguyen, M.; Hammer, T.; Koster, G.; Rijnders, G.; ten Elshof, J. E. Synthesis of KCa2Nb3O10 Crystals with Varying Grain Sizes and Their Nanosheet Monolayer Films As Seed Layers for PiezoMEMS Applications. *ACS Appl. Mater. Interfaces* **2015**, 7 (49), 27473−27478.

(56) Qiao, L.; Bi, X. F. Strain state, microstructure and electrical transport properties of LaNiO3films grown on Si substrates. *J. Phys. D: Appl. Phys.* **2008**, 41 (19), 195407.

(57) Wei, H.; Jenderka, M.; Grundmann, M.; Lorenz, M. LaNiO3 films with tunable out-of-plane lattice parameter and their strain-related electrical properties. *Phys. Status Solidi A* **2015**, 212 (9), 1925−1930.

(58) Springholz, G.; Frank, N.; Bauer, G. The origin of surface roughening in lattice-mismatched Frank van der Merwe type heteroepitaxy. *Thin Solid Films* **1995**, 267 (1), 15−23.

(59) Weber, A.; M, V. Nucleus formation in supersaturated systems. *Z. Phys. Chem.* **1926**, 119, 277.

(60) Stranski, I. N.; Krastanov, L. Theory of orientation separation of ionic crystals. *Sitzungsber. Akad. Wiss. Wien, Math.-Naturwiss. Kl., Abt. 2B* **1938**, 146, 797.

(61) Wang, J.; Salm, C.; Houwman, E.; Nguyen, M.; Schmitz, J. Humidity and polarity influence on MIM PZT capacitor degradation and breakdown. *Proceedings of the 2016 IEEE International Integrated Reliability Workshop, IIRW 2016* **2016**, 65−68.

(62) Lee, J.; Choi, C. H.; Park, B. H.; Noh, T. W.; Lee, J. K. Built-in voltages and asymmetric polarization switching in Pb(Zr,Ti)O3 thin film capacitors. *Appl. Phys. Lett.* **1998**, 72 (25), 3380−3382.

(63) Kartawidjaja, F. C.; Sim, C. H.; Wang, J. Ferroelectric and dielectric behavior of heterolayered PZT thin films. *J. Appl. Phys.* **2007**, 102 (12), 124102.

(64) Schenk, T.; Hoffmann, M.; Ocker, J.; Pešić, M.; Mikolajick, T.; Schroeder, U. Complex Internal Bias Fields in Ferroelectric Hafnium Oxide. *ACS Appl. Mater. Interfaces* **2015**, 7 (36), 20224−20233.

(65) Fengler, F. P. G.; Pešić, M.; Starschich, S.; Schneller, T.; Künneth, C.; Böttger, U.; Mulaosmanovic, H.; Schenk, T.; Park, M. H.; Nigon, R.; et al. Domain Pinning: Comparison of Hafnia and PZT Based Ferroelectrics. *Adv. Electron. Mater.* **2017**, 3 (4), 1600505.

(66) Kim, H. J.; Park, M. H.; Kim, Y. J.; Lee, Y. H.; Moon, T.; Kim, K. D.; Hyun, S. D.; Hwang, C. S. A study on the wake-up effect of ferroelectric Hf0.5Zr0.5O2 films by pulse-switching measurement. *Nanoscale* **2016**, 8 (3), 1383−1389.

(67) Zhang, L.; Chen, J.; Zhang, J.; Wang, H.; Xu, L.; Xing, X. Domain-reorientation-induced polarization wake-up of PbTiO3 based ferroelectric thin films. *Ceram. Int.* **2016**, 42 (16), 19212−19217.

(68) Zhou, D.; Xu, J.; Li, Q.; Guan, Y.; Cao, F.; Dong, X.; Müller, J.; Schenk, T.; Schröder, U. Wake-up effects in Si-doped hafnium oxide ferroelectric thin films. *Appl. Phys. Lett.* **2013**, 103 (19), 192904.

(69) Fengler, F. P. G.; Pešić, M.; Starschich, S.; Schneller, T.; Böttger, U.; Schenk, T.; Park, M. H.; Mikolajick, T.; Schroeder, U. Comparison of hafnia and PZT based ferroelectrics for future non-volatile FRAM applications. *2016 46th European Solid-State Device Research Conference (ESSDERC)*, Sept 12−15, 2016; pp 369−372.

(70) Kohli, M.; Muralt, P.; Setter, N. Removal of 90° domain pinning in (100) Pb(Zr0.15Ti0.85)O3 thin films by pulsed operation. *Appl. Phys. Lett.* **1998**, 72 (24), 3217−3219.

(71) Tan, C.; Ouyang, J.; Zhong, X.; Wang, J.; Liao, M.; Gong, L.; Ren, C.; Zhong, G.; Zheng, S.; Guo, H.; et al. Crystallographically

engineered hierarchical polydomain nanostructures in perovskite ferroelectric films. *Acta Mater.* **2019**, *171*, 282−290.

(72) Zhu, K.; Song, B.; Ge, G.; Lin, J.; Yan, F.; Xu, L.; Yan, H.; Shen, B.; Zhai, J.; Chou, X. Construction of multi-domain coexistence enhanced piezoelectric properties of Bi0.5Na0.5TiO3-based thin films. *Journal of the European Ceramic Society* **2021**, *41* (13), 6456−6464.

(73) Zhu, K.; Ge, G.; Yan, F.; Lin, J.; Bai, H.; Li, G.; Jiang, H.; Shen, B.; Zhai, J.; Chou, X. Morphotropic Relaxor Boundary Construction Highly Boosts the Piezoelectric Properties of Bi-Based Lead-Free Thin Films. *ACS Appl. Mater. Interfaces* **2022**, *14* (6), 8115−8125.

(74) Tagantsev, A. K.; Stolichnov, I.; Colla, E. L.; Setter, N. Polarization fatigue in ferroelectric films: Basic experimental findings, phenomenological scenarios, and microscopic features. *J. Appl. Phys.* **2001**, *90* (3), 1387−1402.

(75) Lo, V. C. Modeling the role of oxygen vacancy on ferroelectric properties in thin films. *J. Appl. Phys.* **2002**, *92* (11), 6778−6786.

(76) Jin, H. Z.; Zhu, J. Size effect and fatigue mechanism in ferroelectric thin films. *J. Appl. Phys.* **2002**, *92* (8), 4594−4598.

(77) Yang, S. M.; Kim, T. H.; Yoon, J.-G.; Noh, T. W. Nanoscale Observation of Time-Dependent Domain Wall Pinning as the Origin of Polarization Fatigue. *Adv. Funct. Mater.* **2012**, *22* (11), 2310−2317.

(78) Scott, J. F.; Dawber, M. Oxygen-vacancy ordering as a fatigue mechanism in perovskite ferroelectrics. *Appl. Phys. Lett.* **2000**, *76* (25), 3801−3803.

(79) Dawber, M.; Scott, J. F. A model for fatigue in ferroelectric perovskite thin films. *Appl. Phys. Lett.* **2000**, *76* (8), 1060−1062.

(80) Chopra, A.; Bayraktar, M.; Nijland, M.; Elshof, J. E. t.; Bijkerk, F.; Rijnders, G. Polarization recovery in lead zirconate titanate thin films deposited on nanosheets-buffered Si (001). *AIP Adv.* **2016**, *6* (12), 125209.

(81) Lou, X. J.; Zhang, M.; Redfern, S. A. T.; Scott, J. F. Fatigue as a local phase decomposition: A switching-induced charge-injection model. *Phys. Rev. B: Condens. Matter Mater. Phys.* **2007**, *75* (22), 224104.

(82) Wu, M.; Li, W.; Li, J.; Wang, S.; Li, Y.; Peng, B.; Huang, H.; Lou, X. Fatigue mechanism verified using photovoltaic properties of Pb(Zr0.52Ti0.48)O3 thin films. *Appl. Phys. Lett.* **2017**, *110* (13), 133903.

(83) Lou, X. J. Why do antiferroelectrics show higher fatigue resistance than ferroelectrics under bipolar electrical cycling? *Appl. Phys. Lett.* **2009**, *94* (7), 072901.

(84) Lou, X. J.; Zhang, M.; Redfern, S. A. T.; Scott, J. F. Local Phase Decomposition as a Cause of Polarization Fatigue in Ferroelectric Thin Films. *Phys. Rev. Lett.* **2006**, *97* (17), 177601.

(85) Do, M. T.; Gauquelin, N.; Nguyen, M. D.; Wang, J.; Verbeeck, J.; Blom, F.; Koster, G.; Houwman, E. P.; Rijnders, G. Interfacial dielectric layer as an origin of polarization fatigue in ferroelectric capacitors. *Sci. Rep.* **2020**, *10* (1), 7310.

(86) Schenk, T.; Yurchuk, E.; Mueller, S.; Schroeder, U.; Starschich, S.; Böttger, U.; Mikolajick, T. About the deformation of ferroelectric hystereses. *Appl. Phys. Rev.* **2014**, *1* (4), 041103.

(87) Li, F.; Jin, L.; Xu, Z.; Zhang, S. Electrostrictive effect in ferroelectrics: An alternative approach to improve piezoelectricity. *Appl. Phys. Rev.* **2014**, *1* (1), 011103.